Combustion and Flame 157 (2010) 2211–2221

Contents lists available at ScienceDirect

Combustion and Flame

journal homepage: www.elsevier.com/locate/combustflame

On flame kernel formation and propagation in premixed gases

Kian Eisazadeh-Far [a,*], Farzan Parsinejad [b], Hameed Metghalchi [a], James C. Keck [c]

[a] Northeastern University, Mechanical and Industrial Engineering Department, Boston, MA 02115, USA
[b] Chevron Oronite Company LLC, Richmond, CA 94801, USA
[c] Massachusetts Institute of Technology, Cambridge, MA 02139, USA

ARTICLE INFO

Article history:
Received 14 May 2010
Received in revised form 27 June 2010
Accepted 15 July 2010
Available online 10 August 2010

Keywords:
Flame kernel
Plasma
Laminar burning speed
Spark ignition

ABSTRACT

Flame kernel formation and propagation in premixed gases have been studied experimentally and theoretically. The experiments have been carried out at constant pressure and temperature in a constant volume vessel located in a high speed shadowgraph system. The formation and propagation of the hot plasma kernel has been simulated for inert gas mixtures using a thermodynamic model. The effects of various parameters including the discharge energy, radiation losses, initial temperature and initial volume of the plasma have been studied in detail. The experiments have been extended to flame kernel formation and propagation of methane/air mixtures. The effect of energy terms including spark energy, chemical energy and energy losses on flame kernel formation and propagation have been investigated. The inputs for this model are the initial conditions of the mixture and experimental data for flame radii. It is concluded that these are the most important parameters effecting plasma kernel growth. The results of laminar burning speeds have been compared with previously published results and are in good agreement.

1. Introduction

An understanding of the spark ignition process is important for the improving the fuel efficiency and reducing the emissions of IC engines and burners. Prior research carried out over the past several decades by a large number of investigators [1–21] has shown that the ignition process involves three distinct stages. The first stage, which occurs on a time scale of microseconds, involves the formation of a narrow spark channel followed by the formation of an equilibrium plasma kernel with a radius of approximately 0.5 mm and a temperature of 7000 K. The second stage, which occurs on a time scale of milliseconds, involves the subsequent growth of a constant mass plasma kernel of atomic ions and electrons due to the input of additional electrical energy from the ignition system. The third and final stage involves the ignition of the combustible gas mixture surrounding the hot plasma kernel to produce a propagating flame. The first and third stages of this ignition process have been extensively investigated in prior work and a semi quantitative understanding of them has been achieved. Maly and Vogel [1] in a theoretical and experimental study determined that the most important component of spark discharge is the breakdown process. They mentioned that the other processes including arc and glow discharge are less important because their electrical energy is dissipated into the electrodes. Maly [2] and Ziegler et al. [3] studied the formation of lean methane–air flames based on the theories proposed in [1]. They concluded that the best ignition system is the one with highest level of energy and shortest time interval. Sher et al. [4] did a fundamental study on spark formation in air and proposed a model to calculate the spark kernel temperature after breakdown. They concluded that the initial spark kernel is a very high temperature region, but the temperature drops rapidly due to heat dissipation. They determined that beyond a specific limit, the energy of the spark affects only the initial flame kernel radius, and not the temperature. Sher et al. [5–8] applied the proposed model in [4] to study the formation of actual methane–air flames and the effect of variables on the initial flame kernel. They concluded that the spark kernel is grown in two steps. The first, shorter stage consists of a pressure wave emission. This is followed by a longer period, in which diffusion occurs. Initial flame kernel is formed during the second stage in a constant pressure process. They could estimate the burning speed of methane–air flames in early stages [8]. However, the estimation of initial conditions in early stages and other parameters such as initial temperature of the kernel, radiation from hot gas, heat conductivity, and transport properties is challenging. Ko et al. [9,10] theoretically and experimentally studied the spark ignition of propane–air mixtures. They indicated the existence of a critical radius which depends strongly on equivalence ratio. They also showed the importance of spark electrode gap, spark modes (breakdown, arc, and glow), and cathode–anode falls on ignition process. Chen and Ju [11] studied the evolution of the ignition kernel to a flame ball and they concluded that radiation plays a very important role in transition of initial flame kernel to the actual self-sustained flame.

* Corresponding author. Address: Mechanical and Industrial Engineering, 334 Snell Engineering Center, Northeastern University, 360 Huntington Avenue, Boston, MA 02115, USA. Fax: +1 617 373 2921.
E-mail address: kian@coe.neu.edu (K. Eisazadeh-Far).

0010-2180/$ - see front matter © 2010 The Combustion Institute. Published by Elsevier Inc. All rights reserved.
doi:10.1016/j.combustflame.2010.07.016

There are also numerous works which deal with the effect of geometry and type of spark electrodes on kernel characteristics and flame propagation [12–21]. Most of these papers illustrate the importance of energy losses in early stages, minimum initial radius, ignition energy modes and their effects on flame formation.

The purpose of the present paper is to present a quantitative model for the intervening second and third stages of process which study the electrical energy input to plasma, flame kernel formation, and measuring the laminar burning speed.

2. Experimental system

Figure 1a shows the overall experimental system. Experiments were conducted in a cylindrical combustion chamber with an inner diameter and length of 133.35 mm. Figure 1b shows the cylindrical vessel. The combustible mixture was spark-ignited at the center of the chamber using two spark plugs with extended electrodes. Two different sets of electrodes were used to study the effect of electrode geometry on heat loss. They had diameters of 2.54 mm and 0.381 mm. Both of electrodes were of stainless steel. Both sets had a free length of 40 mm and the spark gap was 1.0 mm. Two extended spark electrodes, shown in Fig. 1b, initiate the combustion process from the center.

2.1. Ignition system

An electronic ignition system consists of high voltage capacitor discharge controlled by the data acquisition program which provides a spark with the necessary energy. Ignition system has been designed with variable voltages and capacitors to produce ignition with different energies. Voltage and current across the spark plug gap during the electrical discharge have been measured by a voltage divider.

2.2. Optical system

A Z-type shadowgraph ensemble has been set up to visualize the flame propagation. A high speed CMOS camera (HG-LE, Redlake Inc.) with a capture rate of up to 40,000 frames per second is placed at the focal point of the second mirror. The capture rate and shutter speed of the camera were optimized depending on the burning speed of the mixture and the brightness of the flame. The light source for the optical system is a 10-Watt Halogen lamp with a condensing lens and a pinhole of 0.3 mm in diameter, which provides a sharp and intense illumination throughout the whole system. Additional information about the optical set up can be found in previous works [22–24].

3. Experimental results

3.1. Discharge energy measurements

Figure 2 shows the measured voltages and currents as a function of time for a spark plug in air for maximum and minimum discharge energies (*DE*). The spike which is seen approximately at 5–10 μs shows the breakdown stage preceding the spark discharge. In this stage the gap is bridged by the avalanche of electrons flowing from cathode to anode. Breakdown energy depends on the spike

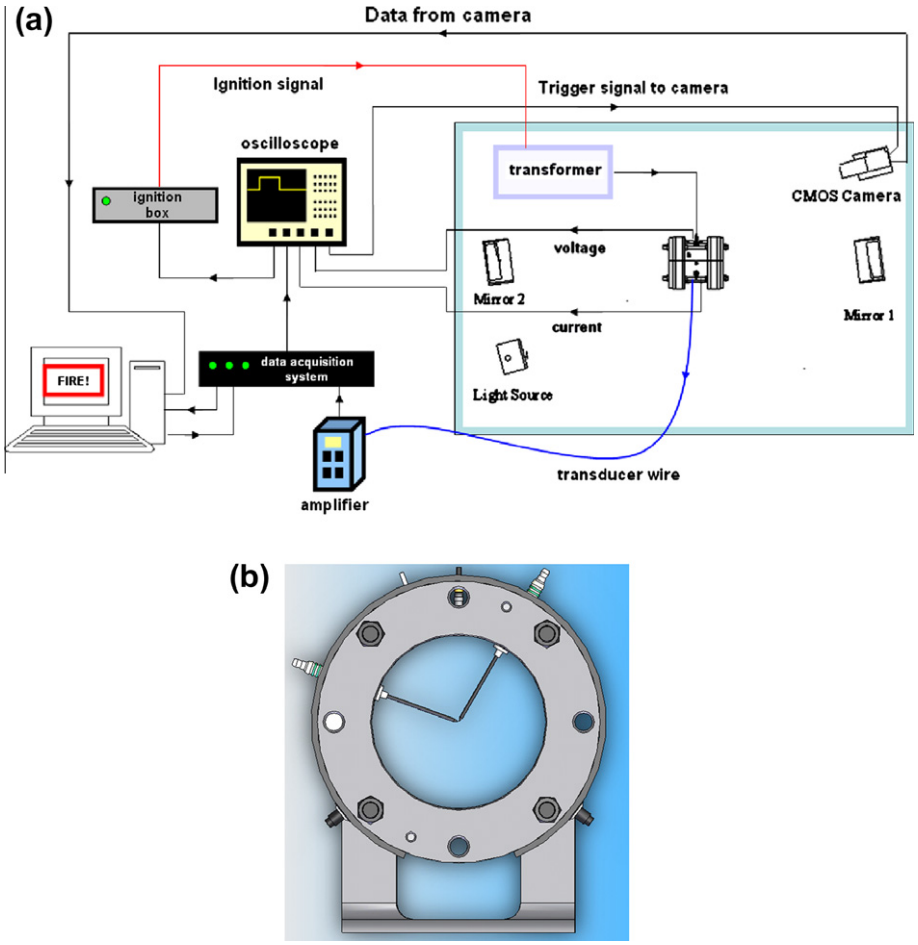

Fig. 1. (a) The experimental set up of the system and (b) cylindrical vessel.

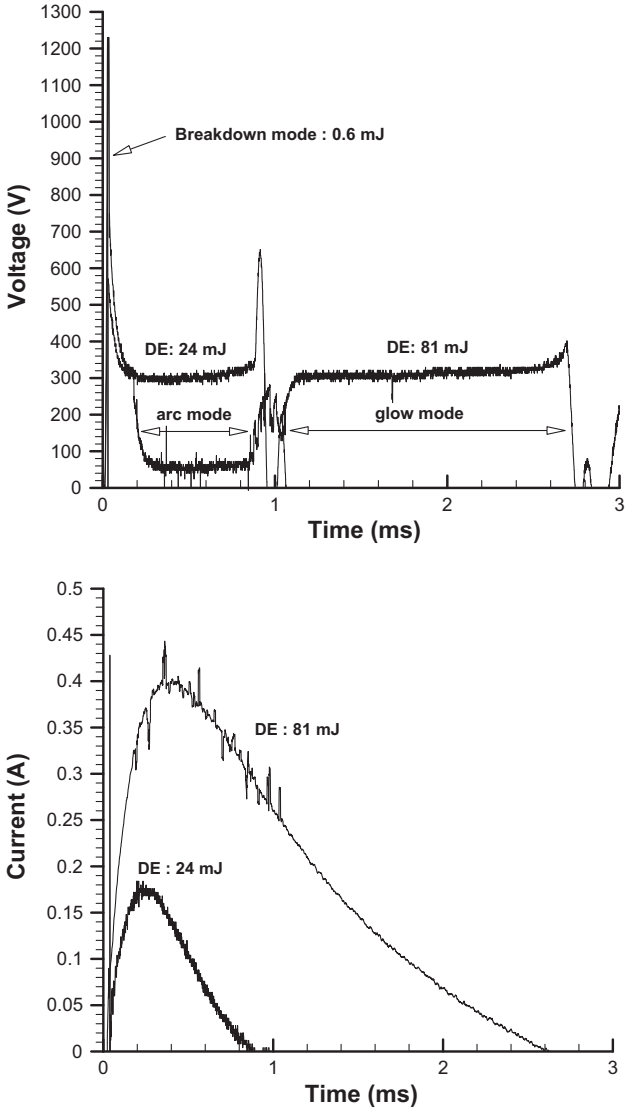

Fig. 2. Voltage and current vs. time for high and low energy: air (arc to glow transition is seen in high energy case).

magnitude and duration of the spark. In our experiments the breakdown energy is about 0.3–0.6 mJ. The oscillations seen starting around 1 ms are feedback through the electrical system. Figure 2 also shows the current flow through the spark plug gap and it can be seen that increasing the discharge energy (*DE*) increases the current flowing across the gap. When the current passes a threshold (~0.3 A) a transition occurs from glow to arc which decreases the voltage abruptly. This transition is caused by thermionic effects causing electron emission from the high temperature cathode. In lower discharge energies, because of relatively low current, there is no arc mode. The glow discharge voltage (normal voltage V_n) is independent of the current. It is a function of wire material and the gas. For air with steel as the electrode material, the value of V_n is 270 volts [2,25,26]. Our experimental observations are very close to these values, as shown in Fig. 2.

Once current and voltage are known as a function of time one can easily calculate the instantaneous discharge power (*DP*) from $DP = VI$. Consequently the discharge energy from the spark jump is $DE = \int VIdt$. Figure 3 shows the instantaneous power across the spark plug gap. For higher energies, there is a sudden drop and rise in the power which is due to the voltage drop in arc-glow transition. It should be noted that discharge energy is larger than the

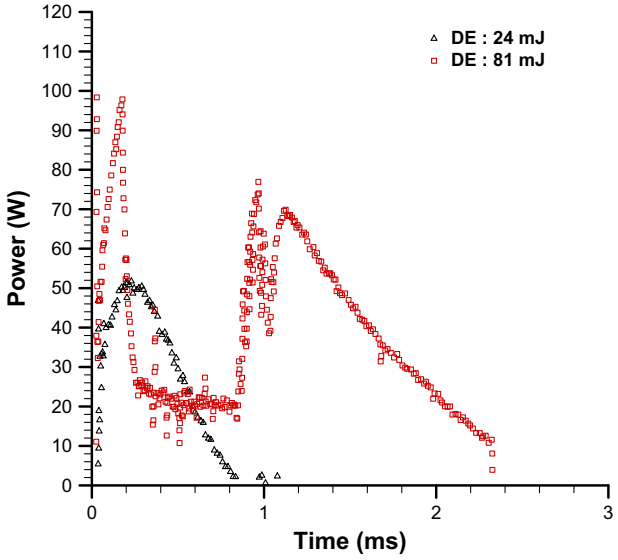

Fig. 3. Spark discharge power of air at low and high energies.

electrical energy converted to thermal energy in the gas because a portion of the discharge energy is dissipated by conduction into the electrodes. It is very difficult to measure the amount of energy dissipated in the plasma but, as will be shown in subsequent sections, a good estimation can be made based the anode and cathode voltage drops measured by others.

3.2. Shadowgraphs of the kernel

Figures 4 and 5 show high speed shadowgraphs of plasma kernels for pure-air and methane/air. As can be seen in Fig. 4, the kernel radii for pure-air and methane/air flames are almost identical at early times. In this stage (0–2 ms), the amount of heat released by chemical reactions is negligible [8]. Therefore, the volume and temperature of the kernel depends only on the electrical energy dissipated in the plasma kernel.

Figure 5 also shows that about 4 ms after spark, the air kernel becomes stable but the methane/air continues to grow into a self-sustained propagating flame. In this stage chemical energy and transport processes are the drivers of flame.

3.3. Kernel growth for air

Figure 6 shows the measured air radii as a function of time for two different spark energies. It can be seen that the kernel radii increase significantly with time independent of discharge energy (*DE*) but the final values increase only slightly with increasing discharge energy (*DE*).

4. Thermodynamic model

A thermodynamic model has been developed to describe the growth of the plasma kernel subsequent to the breakdown phase. Figure 7 shows the sketch of the model.

The major assumptions are as following:

(1) All calculations start after breakdown stage and it is assumed that the pressure is constant.
(2) Since the relaxation time scale of different energy modes (translational, rotational, vibrational, electronic) compared to plasma expansion time are small ($O \sim 10^{-9}$ s), all species are in local thermodynamic equilibrium at a single temperature [1,4,5].

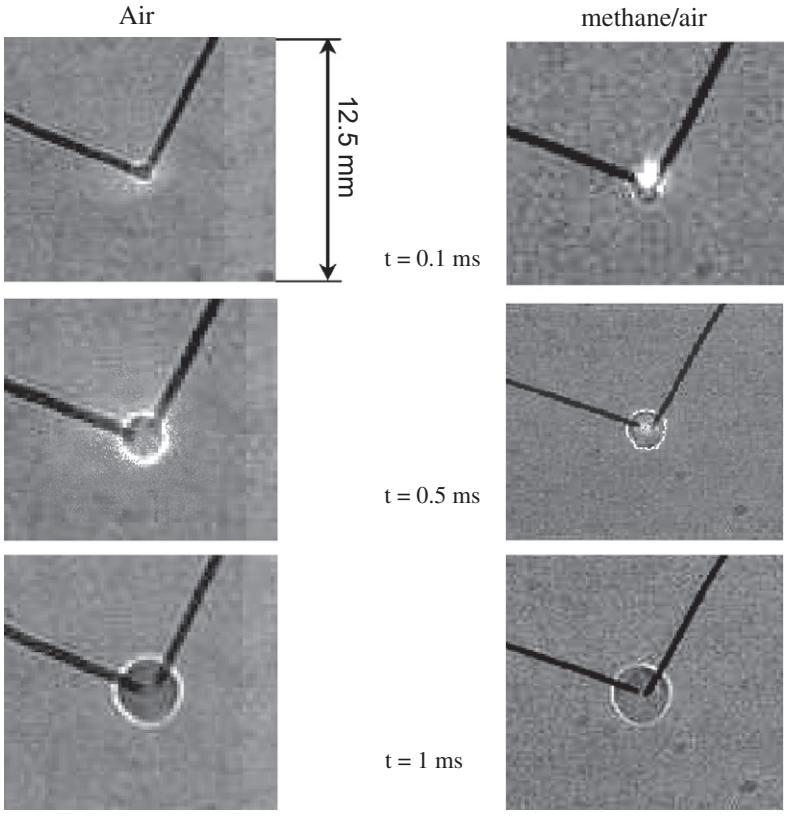

Fig. 4. Snapshots of air and methane/air kernels, P = 1 atm, T = 300 K, discharge energy (DE) = 24 mJ. (*different contrast values of images cause the electrodes appear in different thicknesses*).

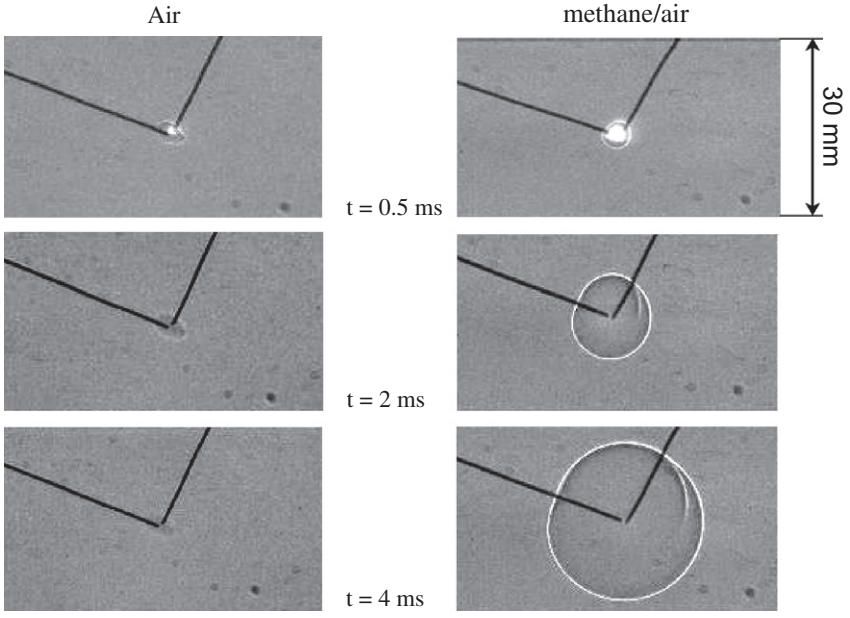

Fig. 5. Snapshots of air and stoichiometric methane/air flame, P = 1 atm, T = 300 K, spark discharge energy (DE) = 24 mJ.

(3) Since the thermal boundary layer is thin, it is assumed that the kernel is a constant-mass system.
(4) It is assumed that the kernel is approximately spherical.
(5) Assumed energy losses are (i) radiation from the plasma to the surroundings, (ii) heat loss associated with anode and cathode voltage drops, and (iii) conduction losses to the thermal boundary layers around the electrodes.

The governing equations are energy balance, equation of state, and mass conservation. The equation for energy balance is given by:

$$\frac{\partial E}{\partial t} = \frac{dDE}{dt} - \dot{Q}_{cond} - \dot{Q}_{rad} - \frac{c_p}{R} p\dot{V} \tag{1}$$

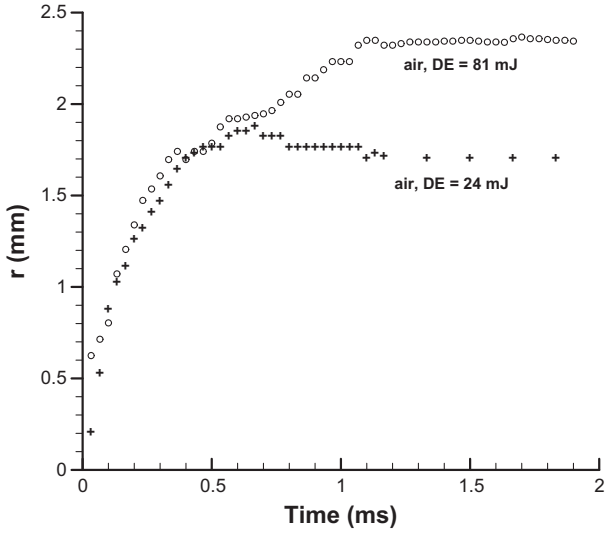

Fig. 6. Air radii at two different spark energies, $P = 1$ atm, $T = 300$ K.

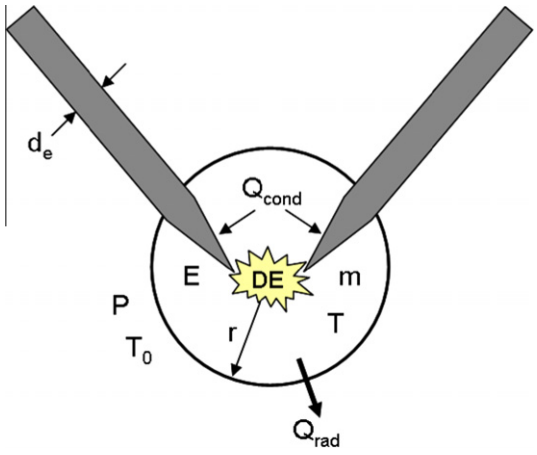

Fig. 7. The sketch of the model.

where E is the energy of the plasma kernel, dDE/dt is the electrical energy dissipation rate, Q_{cond} is the conduction energy loss to the thermal boundary layer, Q_{rad} is the radiation energy loss, c_p is the heat capacity, R is the gas constant, p is the pressure, and $\not{V}$ is the volume of kernel.

The equation of state is

$$p\not{V} = nRT \tag{2}$$

where n is number of moles and T is the temperature. The total number of moles is determined by:

$$n = \sum_{i=1}^{z} n_i \tag{3}$$

where z is the number of species.

The mass conservation equation is

$$EB = 2B_2 + \sum_{\varepsilon=0}^{z} B^{\varepsilon} \quad \varepsilon = 0, 1, 2, 3, \ldots z \tag{4}$$

In this equation, EB is the elemental atom number of atom B, and ε is the charge of ions.

4.1. Thermodynamic properties

The thermodynamic properties of air have been calculated by statistical thermodynamic methods. These parameters, including c_p and the enthalpy of the mixture, have been calculated in temperature range of 300–100,000 K. More details about calculations can be found in [27]. For air the considered species are N_2, N, N^+, N^{2+}, N^{3+}, N^{4+}, N^{5+}, N^{6+}, O_2, O, O^+, O^{2+}, O^{3+}, O^{4+}, O^{5+}, O^{6+}, O^{7+}, and e (electron). Figure 8 shows the number of species for an air plasma normalized by the number of the elemental atoms in the system. It can be seen that the number of species increases rapidly with temperature due to the large increase in the number of electrons at high temperature. Figure 9 shows the heat capacity of air at high temperatures. The peaks in this curve are associated with the energy required to dissociate and ionize the components of air and are responsible for most of its heat capacity.

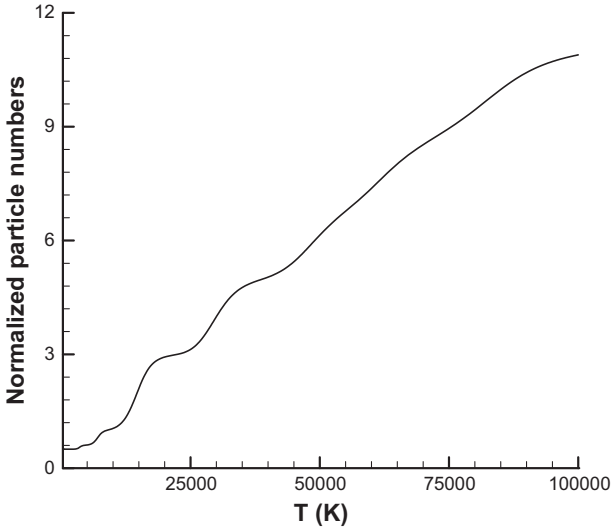

Fig. 8. Particle numbers of air normalized by elemental atom numbers vs. temperature.

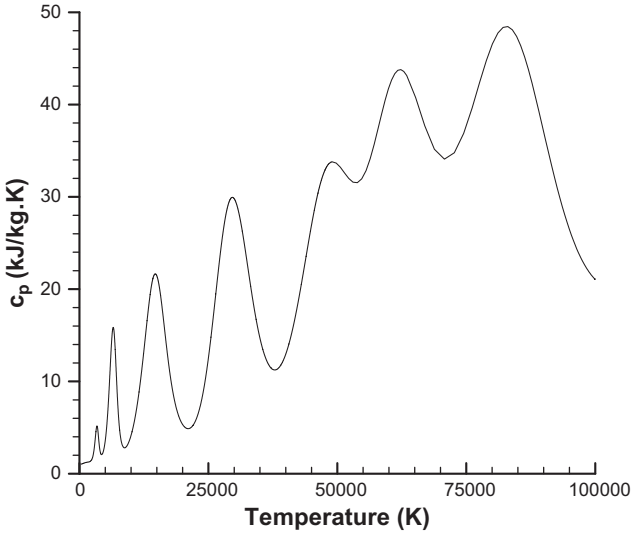

Fig. 9. Heat capacity of air vs. temperature.

4.2. Electrical energy

The calculations start after breakdown phase. A negligible portion of discharge energy is consumed in breakdown phase. Equation. (5) is the discharge energy balance:

$$DE = \int_0^b IVdt + \int_b^t (IV_{fall})dt + \int_b^t (IV_{col})dt = \int_0^b IVdt + Q_{ca} + SE \quad (5)$$

The first term is the energy associated with breakdown, second term is anode and cathode fall energy (Q_{ca}) which is dissipated into the electrodes, and the last term is the electrical energy dissipated within the plasma kernel (SE).

As previously discussed, the experimental data show that breakdown is a very short process ($O \sim 10^{-6}$ s) and its net energy is a small fraction of total energy. After the breakdown phase, arc or glow modes are established (based on the amount of current). In this stage a part of energy is dissipated into the electrodes by conduction. We will show in subsequent sections that in addition to conduction, radiation is an important source of energy losses.

4.3. Conduction to electrodes by thermal boundary layer

Conduction to electrodes was calculated using an unsteady conduction process in the boundary layer. It can be shown that

$$Q_{cond} = 2\int \frac{k_T A_e (T - T_0)}{\sqrt{\alpha t}} dt \quad (6)$$

In this equation k_T is the thermal conductivity of the gas; A_e is the contact area of electrodes with the gas, T_0 is the temperature of the electrode, and α is the thermal diffusivity.

4.4. Effect of initial temperature

Initial temperature of the kernel is important to the ionization process of the kernel. As mentioned before, the calculations start after the emission of the shock wave. The initial temperature of the kernel mainly depends on the breakdown energy and the initial volume of the kernel. Figures 10 and 11 show the effect of initial temperature on kernel growth and temperature. Figure 10 shows that lower initial temperatures result in larger kernel radii, because for a constant volume initial kernel the number of particles is higher for lower initial temperatures. Figure 11 demonstrates that initial temperature affects the temperature profile dramatically. The appropriate range of initial temperature proposed by other researchers is about 6000–7000 K [1,2,4–6].

4.5. Effect of initial radius

Figures 12 and 13 show the effects of initial radius on flame kernel growth and temperature. Initial radius does not have a big influence on the growth rate of the kernel but it has a remarkable effect on the temperature of the kernel. Increasing the initial radii just by 0.05 mm increases the final temperature by about 10,000 K.

4.6. Best fit to the model

The inputs of the model are initial radius, initial temperature, and the spark energy. The initial radius is measured in the experiments by a high resolution camera. The initial temperature of the plasma for air depends on breakdown energy. However, the agreed range among researchers for a wide range of breakdown energies is 6000–7000 K. Table 1 shows the values of initial conditions.

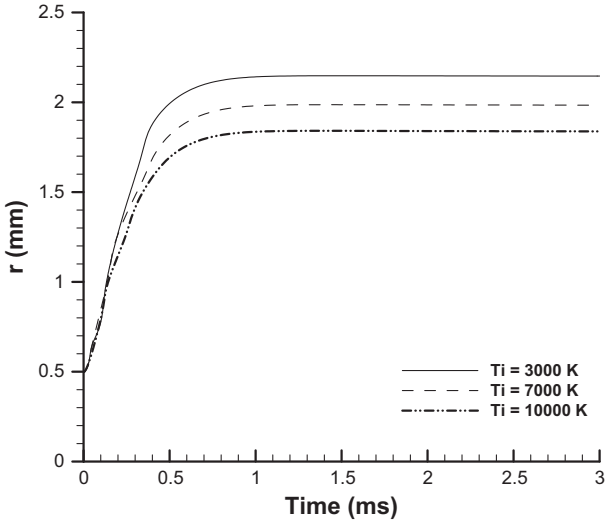

Fig. 10. The effect of initial temperature on air plasma growth, discharge energy = 24 mJ, r_i = 0.5 mm.

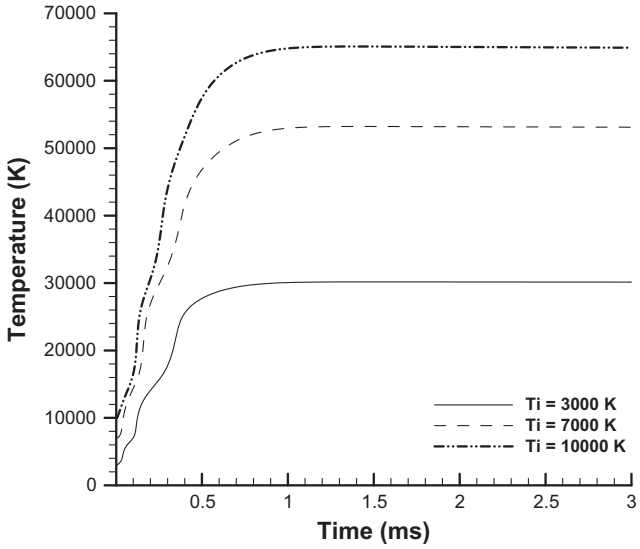

Fig. 11. The effect of initial temperature on air plasma temperature profile, discharge energy = 24 mJ, r_i = 0.5 mm.

Figure 14 shows the comparison between the model and experiment for air. This figure also shows the effect of radiation on predictions of the model. The correlations of air radiation are taken from Schreiber and Hunter [28] who collected data for transport properties of air at high temperatures in optically thin conditions. Experimental data presented in Fig. 14 show a decline in the radii of kernel after a peak which depends on spark power and duration. Figure 14 shows that in zero radiation condition the radius remains constant after the peak. But the addition of the radiation term in equations predicts a decline in radii which is observed in experiments as well. The importance of radiation strongly depends on the temperature. Figure 14b demonstrates that at higher discharge energy, the effect of radiation becomes more important which is due to larger area of the kernel and higher temperature of the plasma. By including radiation term, the predictions show good agreement with experiment. Major terms which control the growth of the kernel are heat capacity, cathode falls and radiation losses.

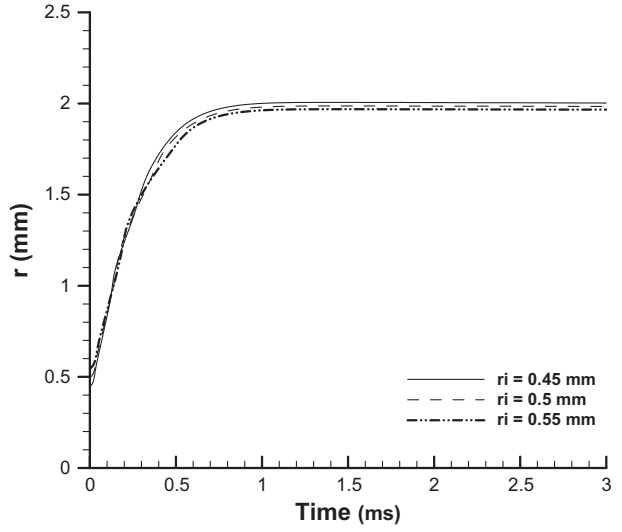

Fig. 12. The effect of initial radius on air kernel growth temperature, T_i = 7000 K, discharge energy = 24 mJ.

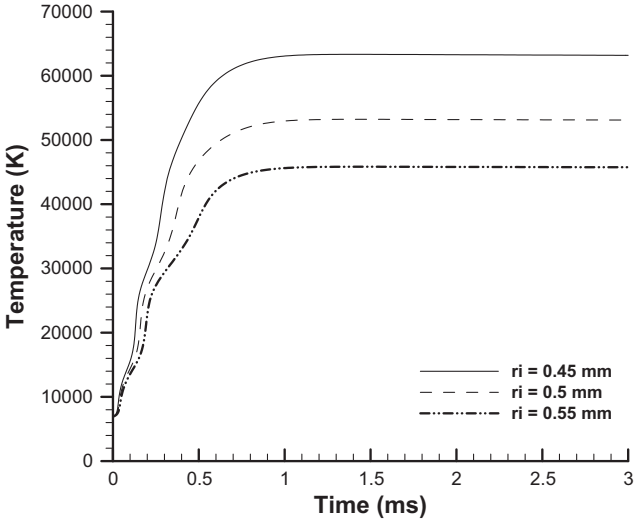

Fig. 13. The effect of initial radius on air kernel temperature, T_i = 7000 K, discharge energy = 24 mJ.

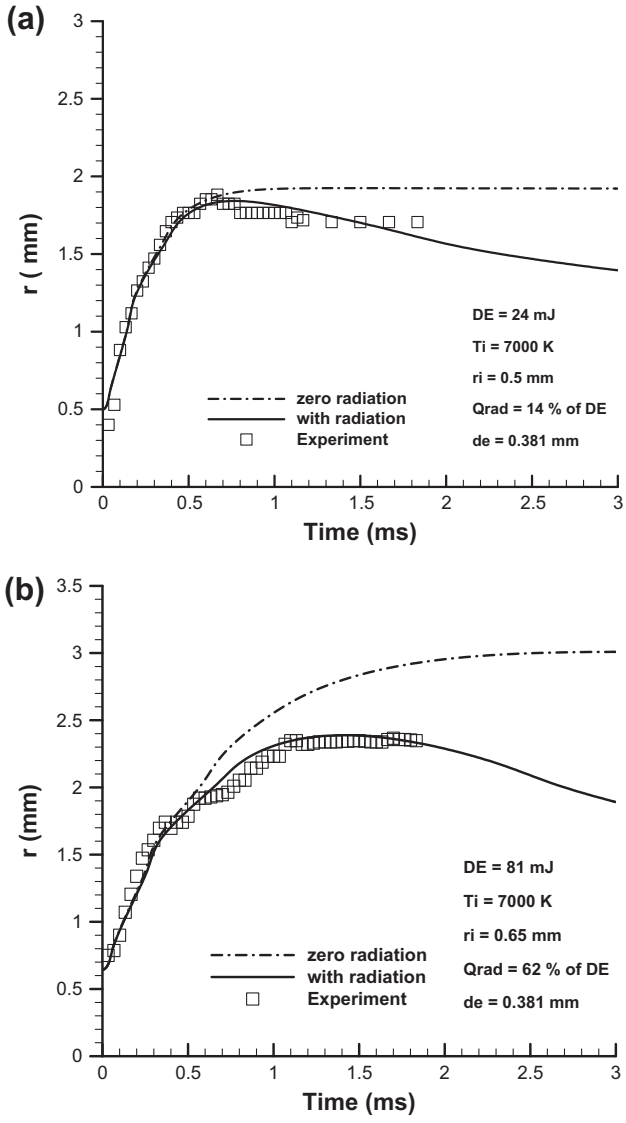

Fig. 14. Predictions of air plasma radii and the comparison with experiments in: (a) low and (b) high discharge energies, P = 1 atm, T = 300 K, symbols: experiment, solid line: model.

Table 1
Initial conditions for calculations.

	Air (*DE* = 24 mJ)	Air (*DE* = 81 mJ)
Initial radius (mm)	0.5	0.65
Initial temperature (K)	7000	7000
DE (mJ)	24	81
SE (mJ)	18	60

4.7. Fraction of total energy losses

Figure 15 shows different energy terms in air kernels. It can be seen that in air plasma, radiation can dissipate 20–60% of discharge energy (*DE*) depending on spark duration and temperature. This percentage strongly depends on the current and the temperature of the arc [29]. The discharge energy (25–30%) is dissipated by the cathode fall conduction and thermal boundary layer dissipations. A small portion of the discharge energy is dissipated by thermal boundary layer around the electrodes. By this token, just about 10–25% of discharge energy is converted to the thermal energy. Although Teets and Sell [30] state that the major part of energy dissipation is due to conduction losses to the electrodes the results are in agreement with net results of Teets and Sell [30] and Maly et al. [1,2]. Table 2 shows the summary of energy dissipations in air.

5. Methane/air mixture

5.1. Flame radius

In this section the growth of methane/air flames will be discussed. The experiments have been done with various equivalence ratios from 0.7 to 1.4. The discharge energies were 24 and 81 mJ and two electrodes were used whose specifications were explained in previous sections. Figure 16 shows the flame radii of the mixtures at stoichiometric condition, low and high variant spark energies, and two different spark electrodes. It is shown that spark electrode geometry does not affect the flame speed. Figure 16b

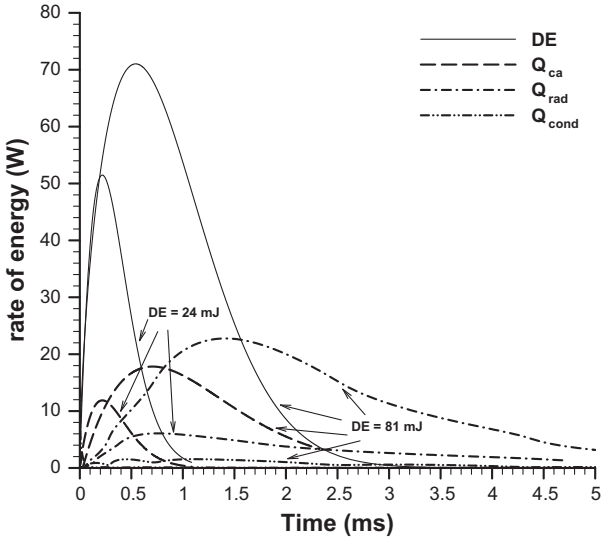

Fig. 15. Rate of variations of discharge energy (DE), cathode–anode fall dissipations (Q_{ca}), radiation losses (Q_{rad}), and conduction dissipations by thermal boundary layer (Q_{cond}) for air, r_i = 0.5 mm, de = 0.38 mm.

Table 2
Summary of fractional energy terms.

	Air (DE = 24 mJ) (%)	Air (DE = 81 mJ) (%)
Cathode–anode fall losses	26.60	26
Thermal boundary layer conduction	0.40	1
Radiation losses	48	62
Converted to thermal energy (present study)	25	11
Converted to thermal energy (Teets and Sell [30])	24	14
Converted to thermal energy (Maly and Vogel [1])	30	

show the effect of spark energy on flame propagation. These figures demonstrate that energy of spark affects the location of flame, but asymptotic flame growth rate is independent.

5.2. Model equations

Figure 17 is the sketch of the model. It is assumed that the flame is spherical and propagates in a constant pressure process. The mass is added to the burned gas region by burning the unburned gas. The mass conservation equation on the flame front is:

$$\frac{\partial m}{\partial t} = \dot{m}_b = \rho_u A S_u [1 - \exp(-t/\tau_c)] \tag{7}$$

where m is the mass of the burned gas zone, $\dot{m}_b$ is the mass burning rate, ρ_u is the density of unburned gas, A is the flame area, S_u is the laminar burning speed, and τ_c is a characteristic time scale. As it will be shown in experimental data the flame speed tends to an asymptotic value after a specific time scale which depends on chemical and thermodynamic properties of the mixture. The exponential term and the corresponding time scale τ_c in Eq. (7) represent this behavior.

The energy balance is given by:

$$\frac{\partial E}{\partial t} = \dot{m}_b(c_{pu}T_u + h_u) + \frac{dSE}{dt} - \dot{Q}_{cond} - \dot{Q}_{rad} - p\dot{\forall} \tag{8}$$

$$E = m(c_{vb}T_b + h_b) \tag{9}$$

where E is the energy of the burned gas region, h is the enthalpy and c_{vb} is the heat capacity at constant volume. $\frac{dSE}{dt}$ is the rate of spark energy variations inside the plasma.

The equation of state is:

$$p = \rho_b R_b T_b = \rho_u R_u T_u \tag{10}$$

where ρ is the density.

Equation (8) can be written as

$$\frac{\partial}{\partial t}\left(\frac{c_{pb}}{R_b} p\forall\right) = \frac{c_{pb}}{R_b} pA\dot{r} = \dot{m}_b c_{pb} T_b + \frac{dSE}{dt} - \dot{Q}_{cond} - \dot{Q}_{rad} \tag{11}$$

Let:

$$\dot{r}_c = \frac{\dot{m}_b R_b T_b}{pA} = \frac{\dot{m}_b R_b T_b}{\rho_u R_u T_u A} = \frac{\rho_u}{\rho_b} S_u (1 - \exp(-t/\tau_c)) \tag{12}$$

$$\dot{r}_{elec} = \frac{R}{c_p}\frac{dSE}{dt}\frac{1}{pA} \tag{13}$$

$$\dot{r}_{cond} = \frac{R}{c_p}\frac{\dot{Q}_{cond}}{pA} \tag{14}$$

$$\dot{r}_{rad} = \frac{R}{c_p}\frac{\dot{Q}_{rad}}{pA} \tag{15}$$

In Eqs. (11)–(15), A is the area of the flame and r is the radius of the flame. By dividing Eq. (11) by $\frac{c_{pb}}{R_b} pA$, we will have:

$$\dot{r} = \dot{r}_c + \dot{r}_{elec} - \dot{r}_{cond} - \dot{r}_{rad} \tag{16}$$

In this equation the role of each energy term on flame speed has been involved. In Eq. (16), $\dot{r}_c$ is the flame speed term corresponding to chemical energy, $\dot{r}_{elec}$ is the flame speed term corresponding to electrical energy, and $\dot{r}_{cond}$ and $\dot{r}_{rad}$ are the effects of conduction and radiation energy losses on flame speed. Having experimental data on the radius of flame and electrical energy, the experimental data were fitted by Eq. (16). The achieved parameters after fitting are S_u and τ_c. Figure 18 shows the flame speed values measured by experiments and fitted by the model. The symbols represent the experimental data. The fluctuations in early stages are associated with the oscillations of heat capacity in early stages which affects the dynamics of the kernel. Later on, the oscillations are due to acoustic waves. In Fig. 18 the effect of other terms presented in Eq. (16) is also shown. High flame speed values in the beginning are due to very high temperature plasma gas. In almost all cases radiation plays an important role in early stages due to the emission of high temperature gas. Figure 18 indicates that chemical energy term has an exponential behavior and it takes time to become asymptotic. Experimental data from Dreizler et al. [31] show that deposition of chemical energy in the kernel begins in the early stages of flame formation but in the first 2 ms the energy supply is dominated by electrical energy. The amount of energy supplied by electrical energy is almost three orders of magnitude higher than the chemical energy. After 2 ms the electrical energy is eliminated and the chemical energy becomes the driver of the flame. Based on conditions, laminar flame becomes asymptotic ultimately. In early stages of ignition the flame speed is more dominated by expansion of the plasma kernel which is a constant pressure and mass process. The experimental data verify this theory as well. Figure 5 shows that in early stages the radii of air and methane/air mixture do not differ dramatically. The transition process from constant mass expansion to the actual self-sustained flame is a complicated process and it depends on the properties of the mixture, energy loss processes, mass and heat diffusion and the rate of chemical reactions. However, the chemical energy time scale τ_c can quantitatively show the transition duration. Table 3 shows the values of S_u and τ_c at two different spark energies and spark electrodes. It is shown that the laminar burning speed is almost

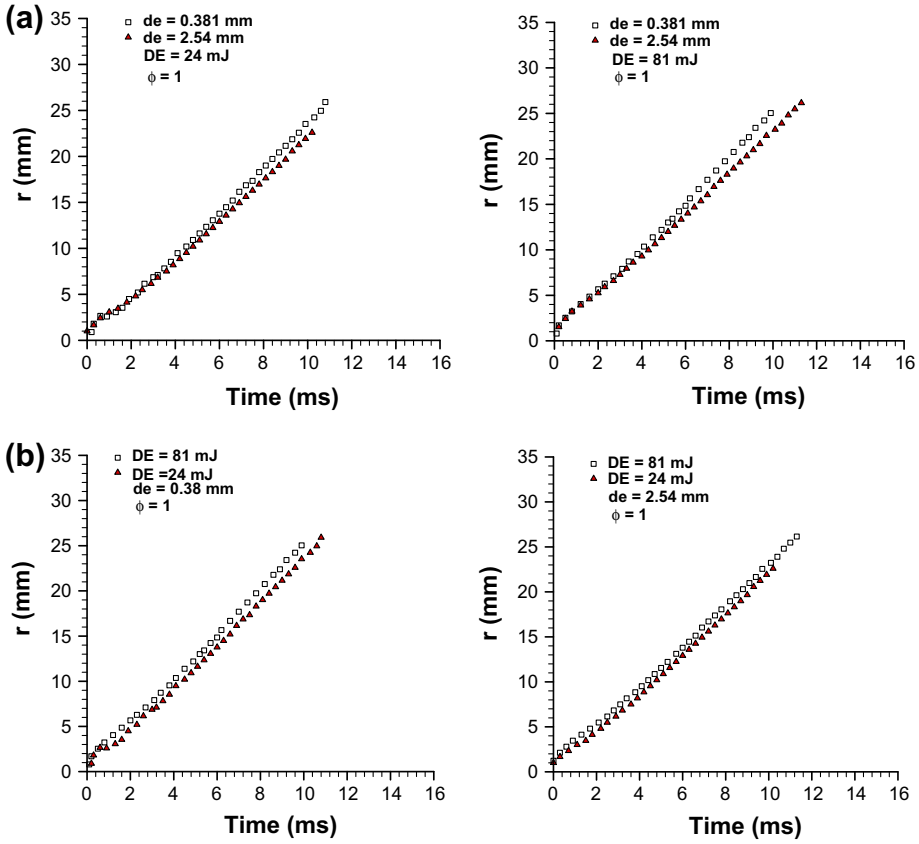

Fig. 16. Flame radii of methane/air mixtures at two different spark energies and electrodes, $P = 1$ atm, $T = 300$ K, $\phi = 1$: (a) effect of discharge energy and (b) effect of electrode geometry.

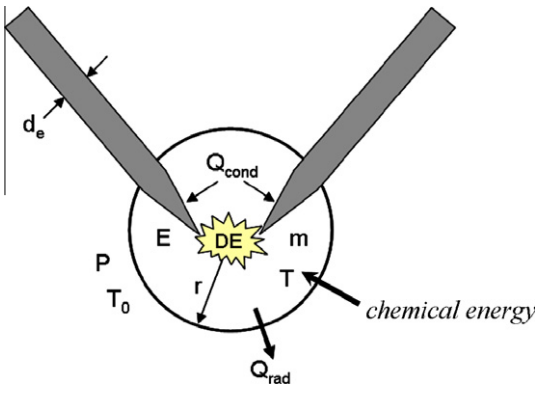

Fig. 17. Schematic of flame propagation model.

independent of spark energy and electrode geometry. The slight difference in results can be attributed to experimental errors.

6. Errors and uncertainties

The sources of experimental uncertainty can be errors in preparation and filling the vessel by methane/air mixture, different discharge energies, and software errors in measuring the radii. Our analyses in previous publications prove that errors due to mixture stoichiometry are ~1% [22–24]. The data have been collected with high resolution and high frame per second to minimize the errors of radii measurement which is ~0.5%. Each experiment was performed at least three times at each operational condition. According to statistical methods, three identical runs are sufficient in order to ensure that the confidence level of the experiment is above 95% [32]. By this procedure and considering the human errors, the experimental uncertainties are minimized to less that 5%. The errors in calculations can be due to laminar burning speed fittings and taking derivative of radii data vs. time. However, these errors never exceed 1%.

7. Comparison with other experimental data

The laminar burning speeds of methane/air flames have been measured by several researchers [33–38]. The experimental and theoretical data shown in Fig. 19 have been obtained by different experimental methods. Figure 19 shows the comparison of present results with other experimental and theoretical data. Our measurements are in good agreement with other data. However, the discrepancy among the data can be associated with experimental errors and different techniques used for measurements. These discrepancies increase in the vicinity of ignition limits at lean and rich conditions (0.7 and 1.3).

8. Summary and conclusions

An experimental and theoretical study was done on flame kernel formation and propagation of premixed gases. The formation of hot plasma during the spark discharge was studied experimentally and a thermodynamic model was developed for air plasma. The effect of various parameters on plasma kernel formation and propagation were studied. The major conclusions are as follows:

(1) A major part of discharge energy is dissipated by cathode fall energy losses. The amount of dissipated cathode fall energies depends on the amount and duration of discharge energy.

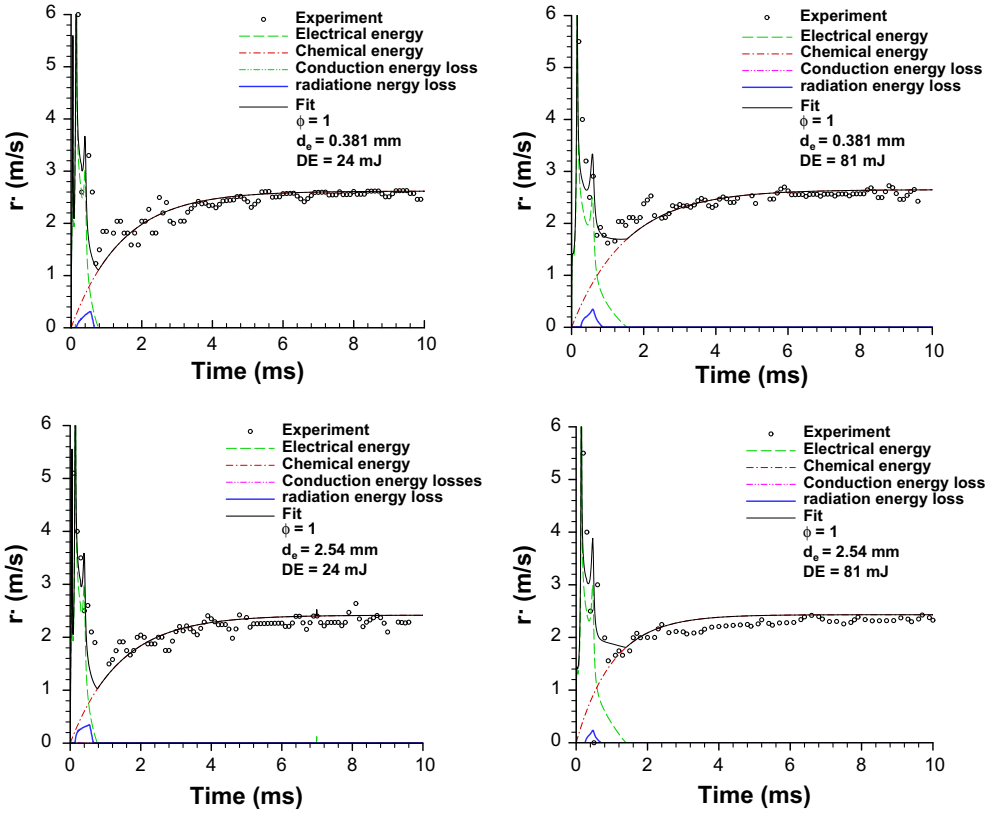

Fig. 18. Flame speeds of methane/air mixtures and the effect of other terms, $P = 1$ atm, $T = 300$ K, $\phi = 1$.

Table 3
Summary of results.

	$DE = 24$ mJ $\phi = 0.8$	$DE = 81$ mJ $\phi = 0.8$	$DE = 24$ mJ $\phi = 1$	$DE = 81$ mJ $\phi = 1$	$DE = 24$ mJ $\phi = 1.2$	$DE = 81$ mJ $\phi = 1.2$
S_u (cm/s)						
$de = 0.38$ mm	22	23	35.7	36	33.1	32.8
$de = 2.54$ mm	24.2	23.5	35.6	34.8	32.8	32.2
τ_c (ms)						
$de = 0.38$ mm	1	1.5	1.4	1.5	4.24	2.5
$de = 2.54$ mm	2.8	2	1.4	1.02	5	1.07

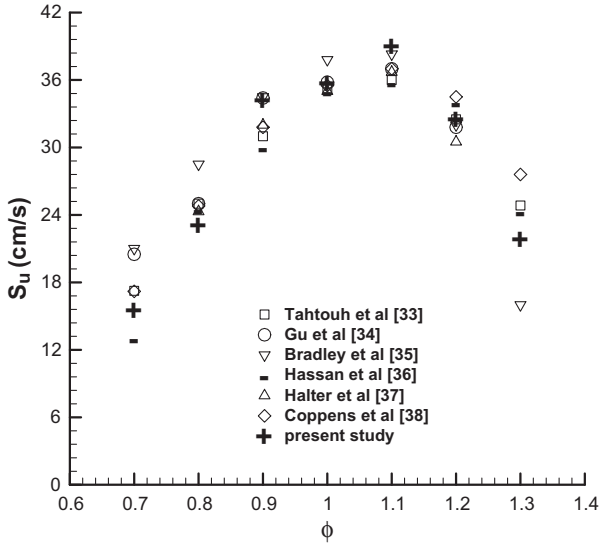

Fig. 19. Laminar burning speeds vs. equivalence ratio and comparison with other experimental data, $P = 1$ atm, $T = 300$ K.

Radiation is the important source of energy losses in plasma. The amount of radiation energy loss strongly depends on the temperature of the hot plasma. However, when self-sustained flame establishes radiation is not an important source of energy loss. Only about 10–25% of the, electrical energy is converted to thermal energy.

(2) It was concluded that the plasma expands in a constant mass and pressure process with increasing number of moles due to ionization.

(3) Increase in heat capacity at high temperatures is an important factor in dynamics and temperature rise in the kernel.

(4) Initial temperature and initial volume of the kernel are important parameters in growth and temperature of the plasma kernel.

(5) The amount of electrical energy input is important to the size and temperature of the kernel.

In second part of this study, the propagation of premixed methane/air flames was studied experimentally and theoretically. The experiments were performed on methane/air flames at atmospheric pressure and temperature, with two different spark

electrodes, and two different spark energies. The conclusions are as follows:

(1) The amount of input electrical energy is important in the location of flame but it does not affect the asymptotic flame speed.
(2) The geometry of the spark electrode does not affect the flame speed and location of flame.
(3) The laminar burning speed was measured by this model and it was in good agreement with experimental results of other researchers.
(4) Laminar flame needs a certain amount of time to become self-sustained. This time scale depends on the composition of the mixture and input electrical energy. This time scale increases when the mixture becomes richer.

Acknowledgments

This research has been done by the support of Office of Naval Research (ONR), Grant No. N00010-09-1-0479. The authors are thankful for technical monitoring of Dr. Gabriel Roy.

References

[1] R. Maly, M. Vogel, Proc. Combust. Inst. 17 (1979) 821–831.
[2] R. Maly, Proc. Combust. Inst. 18 (1981) 1747–1754.
[3] G.F.W. Ziegler, E.P. Wagner, R. Maly, Proc. Combust. Inst. 20 (1985) 1817–1824.
[4] E. Sher, J. Ben-Ya'Ish, T. Kravchik, Combust. Flame 89 (1992) 214–220.
[5] E. Sher, J.C. Keck, Combust. Flame 66 (1986) 17–25.
[6] T. Kravchik, E. Sher, Combust. Flame 99 (1994) 635–643.
[7] T. Kravchik, E. Sher, J.B. Heywood, Combust. Sci. Technol. 108 (1995) 1–30.
[8] S. Refael, E. Sher, Combust. Flame 59 (1985) 17–30.
[9] Y. Ko, R.W. Anderson, V.S. Arpaci, Combust. Flame 83 (1991) 75–87.
[10] Y. Ko, V.S. Arpaci, R.W. Anderson, Combust. Flame 83 (1991) 88–105.
[11] Z. Chen, Y. Ju, Combust. Theory Model. 11 (3) (2007) 427–453.
[12] Y.G. Lee, D.A. Grimes, J.T. Boehler, J. Sparrow, C. Flavin, SAE Paper 2000-01-1210.
[13] S. Pischinger, J.B. Heywood, Proc. Combust. Inst. 23 (1991) 1033–1040.
[14] J. Song, M. Sunwoo, SAE Paper 2000-01-0960.
[15] D. Bradley, C.G.W. Sheppard, I.M. Suardjaja, R. Woolley, Combust. Flame 138 (2004) 55–77.
[16] T. Mantel, SAE Paper 920587.
[17] T. Berglind, J. Sunner, Combust. Flame 63 (1986) 279–288.
[18] H.C. Adelman, Proc. Combust. Inst. 18 (1981) 1333–1342.
[19] S.V. Arpacı, Y. Ko, M. Taeck Lim, H.S. Lee, Combust. Flame 135 (2003) 315–322.
[20] J.L. Beduneau, B. Kim, L. Zimmer, Y. Ikeda, Combust. Flame 132 (2003) 653–665.
[21] D.R. Ballal, A.H. Lefebvre, Proc. Combust. Inst. 18 (1981) 1737–1746.
[22] F. Rahim, K. Eisazadeh-Far, F. Parsinejad, R.J. Andrews, H. Metghalchi, H, Int. J. Thermodyn. 11 (2008) 151–161.
[23] K. Eisazadeh-Far, F. Parsinejad, H. Metghalchi, Fuel 89 (2010) 1041–1049.
[24] F. Parsinejad, J.C. Keck, H. Metghalchi, Exp. Fluids. 43 (2007) 887–894.
[25] A. Engel, M. Steenbeck, Elektrische Gasentladungen. Ihre Physik und Technik, vol. II, Springer, Berlin, 1934.
[26] S.C. Brown, Basic Data of Plasma Physics, MIT Press, Cambridge, MA, 1959.
[27] K. Eisazadeh-Far, H. PhD dissertation, Northeastern University, July 2010.
[28] P.W. Schreiber, A.M. Hunter, AIAA J. 11 (6) (1973).
[29] W. Hermann, E. Schade, A. Phys. 233 (1970) 333–350.
[30] R.E. Teets, J.A. Sell, SAE Paper 880204.
[31] A. Dreizler, S. Lindenmaier, U. Maas, J. Hult, M. Aldén, C.F. Kaminski, Appl. Phys. B: Lasers Opt. 70 (2000) 287–294.
[32] William M.K. Trochim, Research Methods Knowledge Base, 2001.
[33] T. Tahtouh, F. Halter, C. Mounaïm-Rousselle, Combust. Flame 156 (2009) 1735–1743.
[34] X.J. Gu, M.Z. Haq, M. Lawes, R. Woolley, Combust. Flame 121 (2000) 41–58.
[35] Derek Bradley, P.H. Gaskell, X.J. Gu, Combust. Flame 104 (1996) 176–198.
[36] M.I. Hassan, K.T. Aung, G.M. Faeth, Combust. Flame 115 (1998) 539–550.
[37] F. Halter, C. Chauveau, N. Djebaïli-Chaumeix, I. Gökalp, Proc. Combust. Inst. 30 (2005) 201–208.
[38] F.H.V. Coppens, J. De Ruyck, A.A. Konnov, Combust. Flame. 149 (2007) 409–417.